Preprints (www.preprints.org) | NOT PEER-REVIEWED | Posted: 12 December 2016 doi:10.20944/preprints201612.0064.v1

Peer-reviewed version available at Remote Sens. 2017, 9, 207; doi:10.3390/rs9030207

Estimation of Downwelling Surface Longwave Radiation under Heavy Dust Aerosol Sky

Chunlei Wang[1,2], Bo-Hui Tang[1,2,*], Hua Wu[1,2],Ronglin Tang[1,2], Zhao-Liang Li[1,2,3]

[1] State Key Laboratory of Resources and Environment Information System (LREIS), Institute of Geographic Sciences and Natural Resources Research, Chinese Academy of Sciences, Beijing 100101, China; E-mails: tangbh@igsnrr.ac.cn(B.-H.T.); wuhua@igsnrr.ac.cn(H.W.); trl_wd@163.com(R.-L.T.)

[2] University of Chinese Academy of Sciences, Beijing 100049, China;

[3] Key Laboratory of Agri-informatics, Ministry of Agriculture/Institute of Agricultural Resources and Regional Planning, Chinese Academy of Agricultural Sciences, Beijing 100081, China; E-mails: lizhaoliang@caas.cn(Z.-L. Li)

* Author to whom correspondence should be addressed: tangbh@igsnrr.ac.cn; Tel.: +86-10-6488-9684.

Abstract: The variation of aerosols, especially dust aerosol, in time and space plays an important role in climate forcing studies. Aerosols can effectively reduce land surface longwave emission and re-emit energy at a colder temperature, making estimation of downwelling surface longwave radiation (DSLR) with satellite data difficult. Using the latest atmospheric radiative transfer code (MODTRAN 5.0), we simulate the outgoing longwave radiation (OLR) and DSLR under different land surface and atmospheric profile conditions. The results show that dust aerosol has an obvious "warming" effect to longwave radiation compared with other aerosols, that aerosol longwave radiative forcing (ALRF) increased with increasing aerosol optical depth (AOD), and that the atmospheric water vapor content (WVC) is critical to the understanding of ALRF. A method is proposed to improve the accuracy of DSLR estimation from satellite data for the skies under heavy dust aerosols. The AOD and atmospheric WVC under cloud-free conditions with a relatively simple satellite-based radiation model that yields the high accurate DSLR under heavy dust aerosol are used explicitly as model input to reduce the effects of dust aerosol on the estimation of DSLR. Validations of the proposed model with satellites data and field measurements show that it estimates the DSLR accurately under heavy dust aerosol skies. The root mean square errors (RMSEs) are 20.4 W/M^2 and 24.2 W/M^2 for Terra and Aqua satellites, respectively, at the Yingke site, and the biases are 2.7 W/M^2 and 9.6 W/M^2, respectively. For the Arvaikheer site, the RMSEs are 23.2 W/M^2 and 19.8 W/M^2 for Terra and Aqua, respectively, and the biases are 7.8 W/M^2 and 10.5 W/M^2, respectively. The proposed method is especially applicable to acquire relatively high accurate DSLR under heavy dust aerosol using MODIS data with available WVC and AOD data.

Keywords: Downwelling surface longwave radiation (DSLR); dust aerosol; aerosol optical depth (AOD); MODIS

1. Introduction

As an important component of global radiation balance, downwelling surface longwave radiation (DSLR) is of major interest for the study of land surface processes and land-atmosphere exchange due to its applicability in hydrology, meteorology and climatology [1, 2]. The DSLR generally has a heat-preservation effect on the earth and is a key variable to clarify the temperature dependency of worldwide ablation rates [3]. DSLR is the result of atmospheric scattering, absorption

Preprints (www.preprints.org) | NOT PEER-REVIEWED | Posted: 12 December 2016 doi:10.20944/preprints201612.0064.v1

Peer-reviewed version available at Remote Sens. 2017, 9, 207; doi:10.3390/rs9030207

and emission in the entire vertical column. The concentrations of atmospheric constituents and the vertical distribution of temperature, water vapor, aerosol and clouds play decisive roles in estimating the DSLR. The DSLR can be accurately calculated with satellite-derived radiation products by utilizing complex radiative transfer models [4].

As acquisition of vertical distribution of temperature, humidity, gaseous constituents and cloud information is difficult, the multispectral radiative transfer model can be used to accurately calculate the DSLR with various input parameters. Several parameterizations have been developed to estimate the DSLR using synoptic observations only. Typically, ground level temperature and humidity are used as parameterization factors for calculation of the DSLR under clear skies. Most of the parameterization schemes are based on empirical relationships between the DSLR and atmospheric temperature, humidity or both, although some are based on radiative transfer theory [5-10]. These empirical schemes can perform well under clear sky conditions, especially in climatic conditions similar to those in which they were derived. However, under heavy dust aerosol conditions, their performance degrades severely unless aerosol-dependent corrections are made. Dust aerosol is considered the main source of troposphere aerosol loading and is a source of great uncertainty in climate change modeling. Dust aerosols vary in time in space, and their concentrations alter the microphysical properties of clouds in a process known as the 'first indirect' effect [11, 12].

Aerosol radiative effects in the shortwave spectral range have been widely investigated [13-20]. In a recent study, Valenzuela et al. [21] obtained the daily averages of the shortwave aerosol radiative forcing (ASRF) at the surface and at the top of the atmosphere (TOA) during desert dust events from 2005 to 2010 in Granada, Spain. The ASRF mean monthly values ranged from-13W/M^2 to -34W/M^2 at the surface and -4W/M^2 to -13W/M^2 at the TOA. The negative values of approximately 9W/M^2 to 21 W/M^2 between the surface and the TOA indicate that desert dust induces a reduction of the net shortwave radiation. This suggests that there is a non-negligible atmospheric absorption of solar radiation that induces a significant warming of the atmosphere. Few studies have investigated the longwave radiative effects associated with desert dust intrusions [22-26]. These works note that, on the daily timescale, the longwave effect may compensate for a large fraction (up to 50%) of the substantial decrease of shortwave irradiance recorded at the surface during desert dust episodes. Thus, most studies related to this relevant issue have been conducted over deserts with heavy aerosol load conditions [27-33].

The frequent occurrence of dust aerosols can exert an influence on the surface longwave radiation fluxes that is comparable to a warming effect caused by the established greenhouse gases and implies that the observed longwave enhancement is climatologically significant. Dust aerosols are effective in reflecting solar shortwave irradiance back to space, thereby "cooling" the global surface [34, 35]. With equivalent particle diameters on the order of several micrometers [36], they can also effectively reduce land surface longwave emission and re-emit energy at a colder temperature, thereby "warming" the earth [37-39]. However, numerical simulation of dust aerosol longwave forcing is difficult due to its high spatio-temporal variation and secondary actions [40]. Estimation of the atmospheric downward longwave irradiance under a heavy dust aerosol sky remains a challenging task.

Prior to MODIS, satellite data were limited to reflectance measurements in one or two channels. There were no attempts to retrieve aerosol content on a global scale, though algorithms were developed for use over vegetation or other dark land cover types. The blue channel of MODIS offers the possibility to extend the derivation of optical thickness over land to additional surfaces. Well-

Preprints (www.preprints.org) | NOT PEER-REVIEWED | Posted: 12 December 2016 doi:10.20944/preprints201612.0064.v1

Peer-reviewed version available at Remote Sens. 2017, 9, 207; doi:10.3390/rs9030207

calibrated measurements from the MODIS sensor are now available for detecting the optical properties of aerosols, enabling examination of the role of aerosols on longwave radiative forcing [41]. As can be seen in Table 1, compared with previous imagers, MODIS has 36 channels with improved spectral, spatial and radiometric resolutions [42] and has been used to identify and retrieve aerosol properties over the global surface [43-45].

The method discussed here employs a relatively simple and computationally efficient formulation that utilizes readily available satellite-derived measurements without the need for a radiative transfer model or profiles of atmospheric states to estimate the DSLR under heavy dust aerosol sky from MODIS data. The sensitivity of the new model was analyzed, and a validation of the new method was conducted using the Watershed Allied Telemetry Experimental Research dataset and Arvaikheer site data. The general idea is firstly attempted to quantify the longwave radiative forcing of dust aerosol using its optical parameters and atmospheric parameters, subsequently, by improving the general clear-sky DSLR (DSLR-GC) estimation models, we generalized a formulation adjust to estimate the DSLR under dust aerosol sky conditions. Section 2 describes the data and test sites used in this study. Section 3 presents the method to derive the DSLR from the TOA radiance and other satellite-derived parameters. The results and sensitivity also other issues related to the proposed model are analyzed in Section 4. Section 5 describes validations of the proposed method applied to MODIS satellite data. Finally, conclusions are given in Section 6.

Table 1. Specifications of MODIS infrared channels: bandwidth (μm), spectral radiance ($W/m^{-2}.sr^{-1}.um^{-1}$), reference temperature (K), and noise-equivalent temperature difference NEΔT (K).

Main purpose	Channel	Bandwidth (μm)	Spectral radiance (and reference temperature) (K)	Required NEΔT (K)
	27	6.535–6.895	1.16 (240)	0.25
Water vapor	28	7.175–7.475	2.18 (250)	0.25
	29	8.400–8.700	9.58 (300)	0.05
Ozone	30	9.580–9.880	3.69 (250)	0.25
Surface/cloud	31	10.780–11.280	9.55 (300)	0.05
temperature	32	11.770–12.270	8.94 (300)	0.05
Temperature	33	13.185–13.485	4.52 (260)	0.25
profile/ cloud-	34	13.485–13.785	3.76 (250)	0.25
top height	35	13.785–14.085	3.11 (240)	0.25
	36	14.085–14.385	2.08 (220)	0.35

2. Data and Test Sites

2.1 TIGR Atmospheric Profiles and Simulated Data

To analyze the longwave radiative forcing of dust aerosol and to develop a model which is available for estimating DSLR under dust aerosol, it is crucial to obtain a dataset that includes a wide range of coincident measurements of DSLR, AOD, surface temperature, and emissivities as well as the channel TOA radiance and outgoing longwave radiation (OLR) simultaneously with the pixel scales. However, it is not easy to synchronously measure such data in field experiments. Therefore, MODTRAN (Moderate Resolution Atmospheric Transmittance and Radiance Code) was used to simulate the DSLR at ground level under different atmospheric profile and land surface conditions, and the corresponding MODIS channel radiances at the TOA were generated [46].

To simulate the TOA radiances under dust aerosol with worldwide atmospheric situations and land surface types, the Thermodynamic Initial Guess Retrieval (TIGR) database

Preprints (www.preprints.org) | NOT PEER-REVIEWED | Posted: 12 December 2016 doi:10.20944/preprints201612.0064.v1

Peer-reviewed version available at Remote Sens. 2017, 9, 207; doi:10.3390/rs9030207

(http://ara.abct.lmd.polytechnique.fr/index.php?page=tigr) which are constructed by the Laboratoire de Meteorologie Dynamique (LMD) represent a worldwide set of atmospheric conditions from polar to tropical atmosphere are used. Because the objective of this study focuses on DSLR retrieval in the presence of dust aerosol in cloud-free skies, only the atmospheric profiles under clear skies are considered. As seen in Fig. 1, sixty atmospheric profiles that can represent the global scale were chosen for our MODTRAN simulations and surface emissivity was obtained from the ASTER spectral library (http://speclib.jpl.nasa.gov/). Since there is no spectral emissivity available beyond the 14 μm wavelength and considering the strong absorption of the atmosphere at spectral wavelengths greater than 14 μm, the surface emissivity used in MODTRAN simulation beyond this wavelength is assumed to be unity.

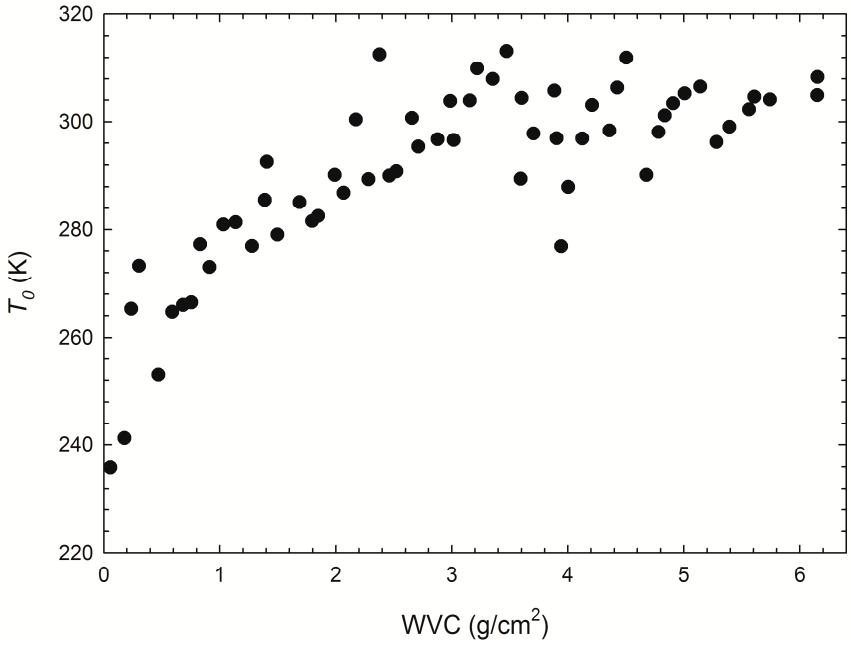

Figure 1. Sixty atmospheric profiles chosen from the TIGR dataset. Scattering diagram of the atmospheric water vapor content (WVC) as a function of the bottom atmosphere temperature (T_0).

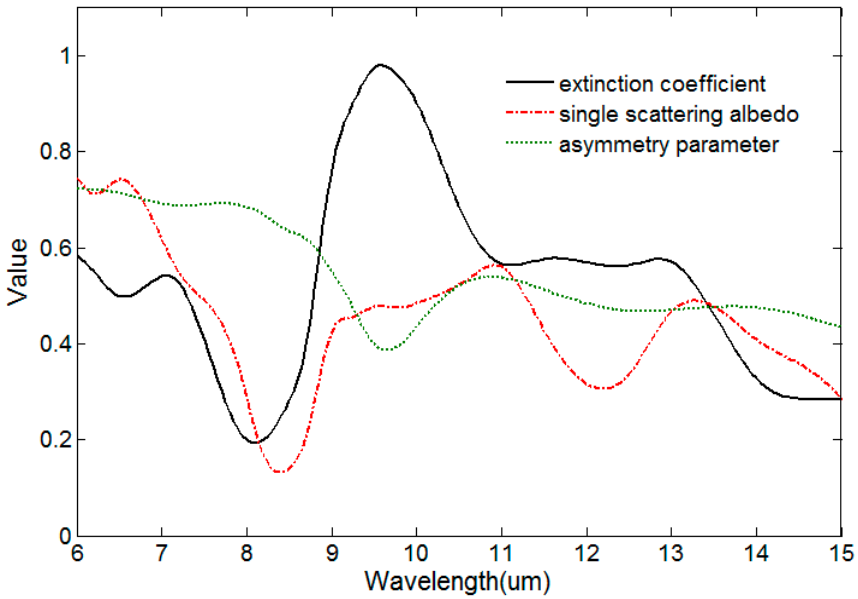

Figure 2. The extinction coefficient, single scattering albedo and asymmetry parameter of dust aerosol at 6 to 15 μm wavelengths.

The optical properties of dust aerosol are acquired from the Optical Properties of Aerosol and Cloud (OPAC) software package [47], which provides the optical properties of different aerosol and

Preprints (www.preprints.org) | NOT PEER-REVIEWED | Posted: 12 December 2016 doi:10.20944/preprints201612.0064.v1

Peer-reviewed version available at Remote Sens. 2017, 9, 207; doi:10.3390/rs9030207

cloud components for wavelengths ranging from visible to TIR and is widely used for general circulation models (GCMs) and climate research. Figure 2 shows the extinction coefficient, single scattering albedo and asymmetry parameter of dust aerosol from 6-15 μm wavelengths. The lowest extinction coefficient and single scattering albedo are in channel 29, which suggests that there is high atmospheric transmittance and weak scattering in this channel wavelength. Channel 30 has the highest extinction coefficient and is greatly influenced by the surface heterogeneity. In channels 31 and 32, the extinction coefficient and asymmetrical parameters are almost identical. From channels 30 to 36, the extinction coefficient and single scattering albedo decrease but the asymmetry parameters basically remain unchanged. Because dust aerosol can significantly reduce the thermal infrared transmittance of the atmospheric window channel [48], our research scope was focused on aerosol optical depth (AOD) less than 1 in 0.55 μm. For comparison, other types of aerosol (rural aerosol, urban aerosol, maritime aerosol) were used in our simulation run.To increase the representativeness, reasonable variations of land surface temperature (LST) were set according to the ground level atmospheric temperature (T_0), which varied from $T_0 - 5$ K to $T_0 + 15$ K in 5 K steps. For the angular dependence of the TOA radiance, six different viewing zenith angles (VZAs) were considered (secant (VZA) = 1.0, 1.2, 1.4, 1.6, 1.8, and 2.0)). After integrating the simulated TOA radiances with the channel response functions of MODIS TIR channels, the MODIS channel radiances were calculated.

2.2 In Situ Measurements and MODIS Satellite Data

Two test sites were used to determine the quality of the improved model. The Yingke (100.406E, 38.854 N) site is in the middle Heihe River Basin in northwest China at an altitude of 1519.1 m and is surrounded by a large and homogeneous corn field. As a relatively ideal proving ground, it is usually covered by dust aerosol and is selected as a test site in our study. The Arvaikheer (46.23N, 102.816E) site in Mongolia is covered by grass and usually affected by dust aerosol from the Gobi Desert. The DSLR in the two radiations were measured using pyrgeometers and sampled on the half hour from January 2007 to December 2009 for the Yingke site and from January 2003 to December 2003 for the Arvaikheer site. Seven MODIS products were are also used:

1) MODIS calibrated radiances (MOD021KM/MYD021KM);
2) MODIS geolocation data (MOD03/MYD03);
3) MODIS aerosol datasets (MOD04_L2/MYD04_L2);
4) MODIS water vapor datasets (MOD05_L2/MYD05_L2);
5) MODIS land surface temperature and emissivity (MOD11_L2/MYD11_L2);
6) MODIS cloud detection product (MOD035_L2/MYD035_L2)
7) Global land surface satellite broadband emissivity product (GLASS BBE).

These products are available in hierarchical data format (HDF); MODIS products are provided by NASA's Goddard Space Flight Center (GSFC) and the Atmosphere Archive and Distribution System (LAADS) (http://ladsweb.nascom.nasa.gov/data/), and the GLASS BBE data is available from the Global Land Cover Facility of the University of Maryland (http://glcf.umd.edu/).

3. Methodology

The paper focuses on the analysis of the influence of dust aerosol on the DSLR and estimation of the DSLR under dust aerosol conditions. The contribution of dust aerosol to the longwave spectral range can be defined as the longwave radiation forcing of aerosol (ALRF). The DSLR is formulated as a simple, physically based bulk expression that accounts for dust aerosol variability. At a given pixel, the formulation describing the DSLR under dust aerosol conditions may be written as the DSLR under clear sky added to the downwelling radiation forcing generated by the dust aerosol.

$$DSLR_{aero} = DSLR_{clr} + ALRF \quad (1)$$

where $DSLR_{aero}$ is the DSLR under dust aerosol conditions and ALRF is the downwelling radiation forcing of dust aerosol. Several models have been developed to estimate the DSLR in clear sky conditions [7-10, 45, 46]. In clear skies, the channel radiance received by the satellite thermal infrared sensor at the TOA is approximately the aggregate of the radiance from the earth's surface and each

Preprints (www.preprints.org) | NOT PEER-REVIEWED | Posted: 12 December 2016 doi:10.20944/preprints201612.0064.v1

Peer-reviewed version available at Remote Sens. 2017, 9, 207; doi:10.3390/rs9030207

level of the atmosphere, when neglecting the scattering of thermal infrared radiation, and it can be expressed as follows [49]:

$$B_i(T_i) = \varepsilon_i B_i(T_s)\tau_i(\theta,\varphi,P_s \to 0) + \int_{P_s}^{0} B_i(T_p)\frac{d\tau_i(\theta,\varphi,P \to 0)}{dInP}dInP + \frac{1-\varepsilon_i}{\pi}\int_0^{2\pi}\int_0^{\pi/2}\int_0^{P_s} B_i(T_p)\frac{d\tau_i(\theta',\varphi',P \to P_s)}{dInP}\cos\theta'\sin\theta' dInP d\theta' d\varphi' \cdot \tau_i(\theta,\varphi,P_s \to 0) \quad (2)$$

where T_i, T_s and T_p are the channel brightness temperature at the TOA, the surface temperature and the air temperature at the level of atmospheric pressure P, respectively. P_s is the atmospheric pressure at ground level, ε_i denotes the surface emissivity, $\tau_i(\theta, \varphi, Ps \to 0)$ is the total atmospheric transmittance along the target-to-sensor path, θ and φ are the viewing zenith and azimuth angles, respectively, and $\tau_i(\theta, \varphi, P \to P_s)$ is the channel's transmittance of the atmosphere from the level of atmospheric pressure P to the ground level (P_s); if $P \to 0$ it is the pressure P to the TOA. The first term is the contribution of the land surface, the second term is atmospheric emission term from all atmospheric levels to the TOA received by the sensor, and the third term represents the corresponding DSLR reflected by the surface and then attenuated by the atmosphere along the path from the surface to the sensor.

Tang and Li [50] introduced an algebraic expression $d\tau_i(P)/d\ln P$ as the channel weighting function that depicts the magnitude of radiance contribution from different atmospheric vertical layers. For MODIS, each weighting function of its TIR channel implies that it can detect information at different altitudes in a vertical atmospheric column. The max value means that this atmosphere level has the maximum magnitude of radiance contributing to the sensor channel radiance. Based on the algebraic expression result of each channel and assuming there is a linear relationship between the DSLR and MODIS channel radiances, for cloud-free and Lambertian surface conditions, Tang and Li [50] developed a new model to retrieve the DSLR directly from the TOA radiances measured by MODIS TIR channels with the formula:

$$DSLR = a_0 + a_1 M_{28} + a_2 M_{29} + a_3 M_{31} + a_4 M_{33} + a_5 M_{34} + a_6 M_{36} \quad (3)$$

$$M_i = \pi \times L_i(\theta) \quad (4)$$

where a_0 to a_6 are the regression coefficients related to VZA and the altitude and $L_i(\theta)$ is the TOA radiance measured by the MODIS TIR channel. The model has been used to estimate the DSLR over the USA and tested at Bondville, Boulder, Desert Rock, Penn State, and Sioux Falls, which represent different surface types. The RMSEs of the linear model are 23.6 W/M²to 39.3 W/M² compared with the measured data at the six sites, considering that the MODIS instrument error is approximately11W/M², its accuracy meets the basic requirements of climate and meteorology prognosis research on DSLR flux. Furthermore, unlike most of the statistical algorithms that need ground-level atmosphere temperature as an input, it estimates the DSLR directly from the TOA radiance and thus was used in our research.

4. Results and Sensitivity Analysis

4.1 Results

According to the definition and the simulation data set, the ALRF under different types and contents of aerosols are shown below.

Preprints (www.preprints.org) | NOT PEER-REVIEWED | Posted: 12 December 2016 doi:10.20944/preprints201612.0064.v1

Peer-reviewed version available at Remote Sens. 2017, 9, 207; doi:10.3390/rs9030207

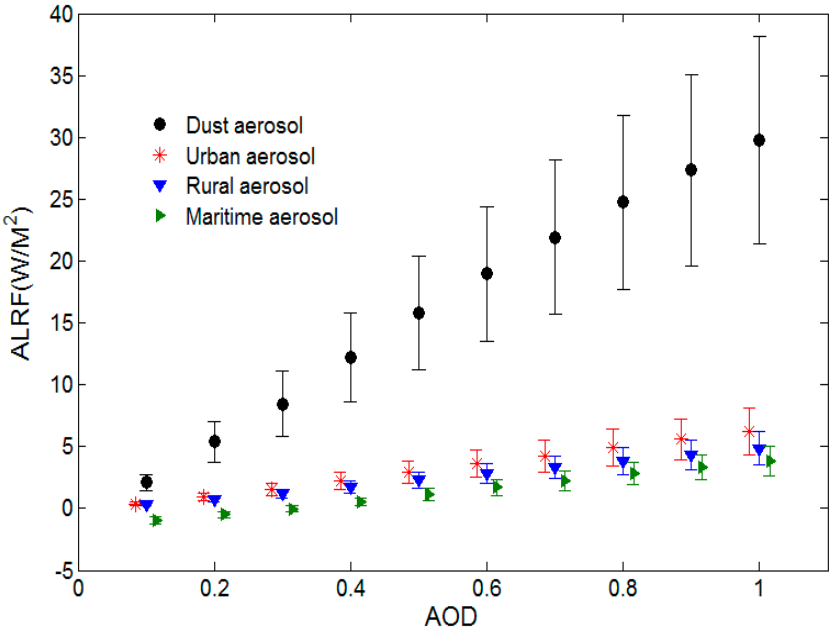

Figure 3. The ALRF of different aerosol types varies with the AOD. The solid symbols indicate the ALRF and the half-length of the vertical bars represents the Standard Deviations of the ALRF.

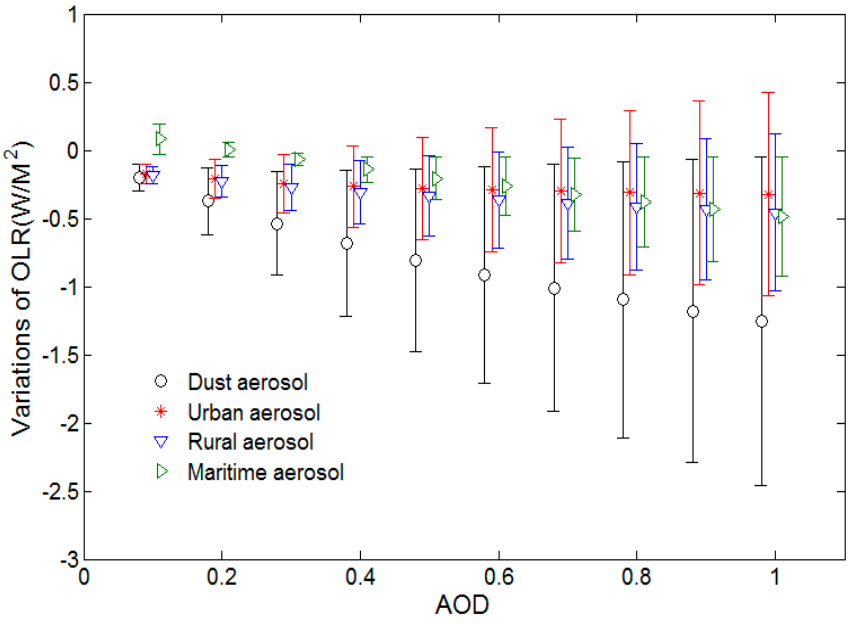

Figure 4. The variations of OLR at different aerosol conditions as the AOD increase. The symbols indicate the variations of OLR and the half-length of vertical bars represent the Standard Deviations of the OLR.

Figure 3 and Figure 4 show the ALRF and OLR influenced by different types and optical depths of aerosols. Notably, dust aerosol has positive effects on the DSLR but negative effects on the OLR, and both effects are enhanced as the AOD increased, the Standard Deviations of the ALRF and OLR also show similar changes. The ALRF of maritime aerosol is relatively small, approximately 3.85 W/M² when the AOD is 1.0, with a Standard Deviations of 1.1 W/M². For rural and urban aerosols, the ALRF is 4.85 W/M² and 6.22 W/M², respectively, with Standard Deviations of 1.32 W/M² and 1.85

Preprints (www.preprints.org) | NOT PEER-REVIEWED | Posted: 12 December 2016 doi:10.20944/preprints201612.0064.v1

Peer-reviewed version available at Remote Sens. 2017, 9, 207; doi:10.3390/rs9030207

W/M², respectively. For dust aerosol, the ALRF increases from 2.09 W/M² to 29.8 W/M² when the AOD increases from 0.1 to 1.0, with Standard Deviations from 0.66 W/M² to 8.3 W/M², respectively. The OLR only changes slightly under the four aerosol types and the max variation is -1.26 W/M² when the AOD=1.0 for dust aerosol.

Moreover, from these figures, we can see that the ALRF of the four aerosol types can be expressed as linear functions of the AOD with coefficients of determination (R^2) of 0.998, 0.998, 0.997 and 0.997. After analyzing the relationships between the ALRF and AOD for other situations, the following linear function can be concluded:

$$ALRF = k \times AOD + b \quad (5)$$

where k and b are the slope and offset, respectively, which vary with the condition of the atmospheric profiles and are determined by the atmospheric water vapor content (WVC), atmospheric temperature, CO_2, O_3 and other constituents.

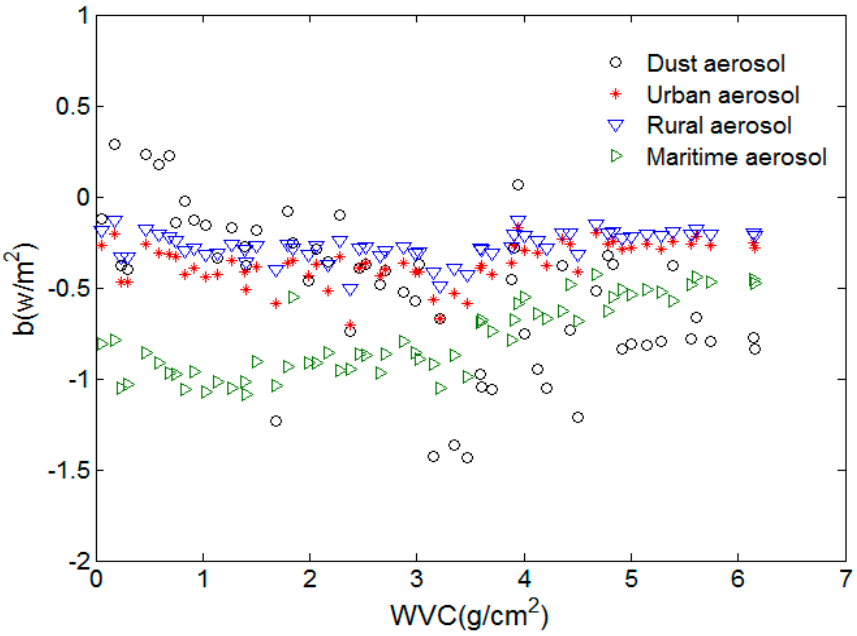

Figure 5. Scattering diagram of offset b in formula (5) as a function of WVC.

Figure 5 shows the scattering diagram of the offset b in formula (5) as function of the WVC. The offset had little variation, from -1.45 to 0.3 for dust aerosol, and can be expressed as constants for aerosol types. Therefore, the ALRF is determined by its slope k, which has a close relationship with the status of the atmosphere. Wang and Liang [51] found that the daily DSLR increased at an average rate of 2.2 W/M² per decade from 1973 to 2008, and that the rising trend has a close relationship with the increasing CO_2 concentration. We researched the influence of CO_2 on the DSLR and the results show that the DSLR has increased 2.0 W/M² as the CO_2 concentration doubled, consistent with the study by Wilson and Gea-Banacloche [52]. The content of CO_2 and other trace gases are steady and relatively small and have a far smaller influence on the DSLR than the WVC.

Thus, the WVC was used to parameterize k and the preliminary result is as follows:

Preprints (www.preprints.org) | NOT PEER-REVIEWED | Posted: 12 December 2016 doi:10.20944/preprints201612.0064.v1

Peer-reviewed version available at Remote Sens. 2017, 9, 207; doi:10.3390/rs9030207

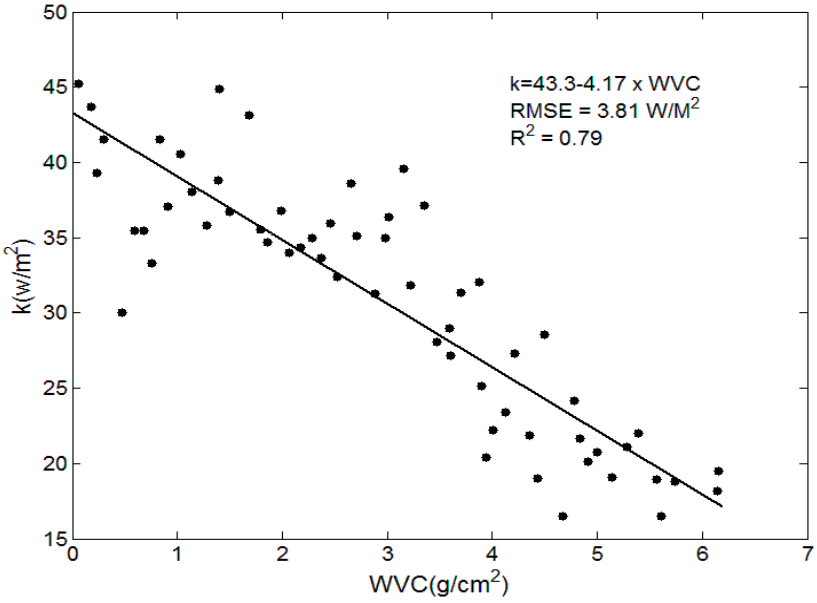

Figure 6. Scattering diagrams of the slope k in formula (5) as a function of atmospheric WVC under dust aerosol type.

For dust aerosol, figure 6 shows the scattering diagrams of the slope k in formula (5) as a function of the atmospheric WVC. If we take the slope k as a linear function of atmospheric WVC, the RMSE is 3.81 W/M² and the determination coefficient (R^2) is 0.79. The ALRF can be roughly calculated with WVC and AOD, so equation (1) can be expressed as:

$$DSLR_{AOD} = DSLR_{clear} + p \times WVC \times AOD + q * AOD + n \quad (6)$$

where $DSLR_{AOD}$ is the DSLR under aerosol sky, $DSLR_{clear}$ is the DSLR in cloud-free sky when no dust aerosol is present and can be estimated with the DSLR-GC model, WVC is the atmospheric water vapor content, AOD is the aerosol optical depth, and p, q and n are regression coefficients. Notably, the coefficients in estimating $DSLR_{clear}$ may have slight variations because of the slight variations in the OLR between heavy dust aerosol and clear sky.

It is well known that the TOA radiance has a close relationship with surface emissivity, which may influence DSLR retrieval. Here, we discussed the accuracy of the improved model on DSLR retrieval for different surface types. Figure7 shows the Root Mean Square Error (RMSE) between the actual DSLR and the model-estimated values for different surface types from VZA = 0° to VZA = 60°. When VZA = 0°, the RMSEs of the proposed model vary from 5.75 W/M² to 8.68 W/M² for different surface types. For VZA =60°, the RMSEs vary from 10.69 W/M² to 12.73 W/M². The RMSE of the improved model generally has a close relationship with the surface type and increased as the VZA increased, which indicates that the model is VZA-dependent.

Preprints (www.preprints.org) | NOT PEER-REVIEWED | Posted: 12 December 2016 doi:10.20944/preprints201612.0064.v1

Peer-reviewed version available at Remote Sens. 2017, 9, 207; doi:10.3390/rs9030207

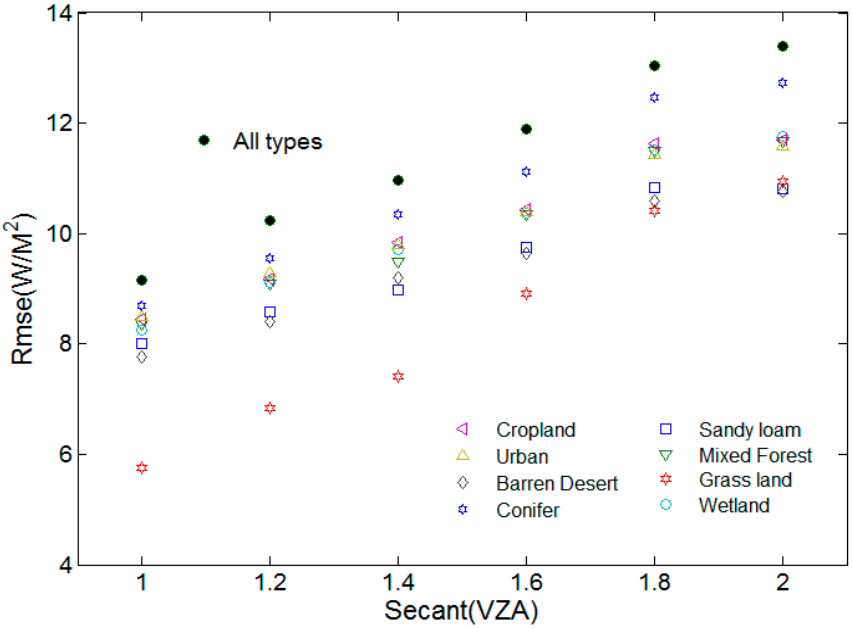

Figure 7. Root mean square error (RMSE) between the actual DSLR (MODTRAN-simulated DSLR) and the DSLR estimated using the proposed models for different surface types from VZA = 0° to VZA = 60° when DEM=0.

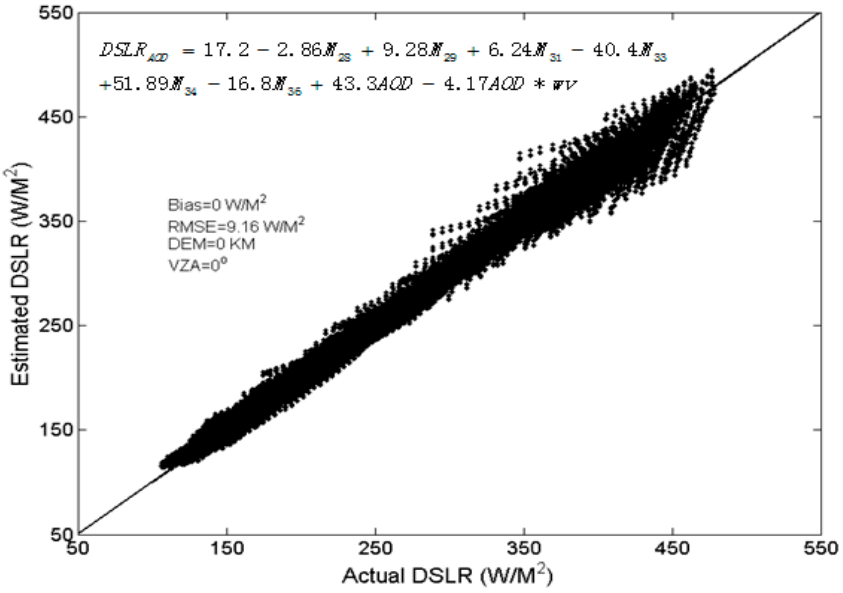

Figure 8. Comparisons of the actual downwelling surface longwave radiation with estimations using the proposed model with the training dataset and VZA=0°, DEM=0 and AOD less than 1.0.

Preprints (www.preprints.org) | NOT PEER-REVIEWED | Posted: 12 December 2016 doi:10.20944/preprints201612.0064.v1

Peer-reviewed version available at Remote Sens. 2017, 9, 207; doi:10.3390/rs9030207

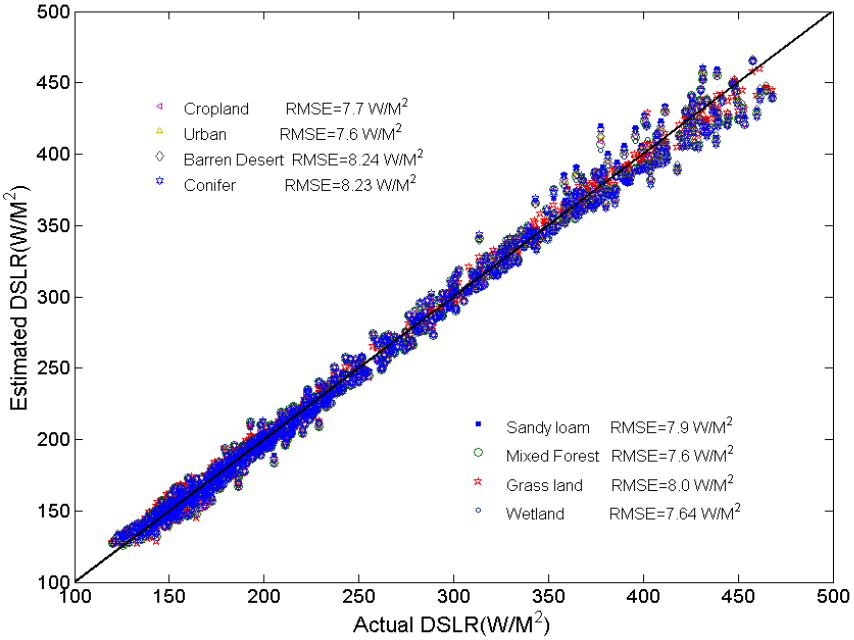

Figure 9. Comparisons of the actual downwelling surface longwave radiation with estimations using the proposed model for different surface types and VZA=0, DEM=0 and AOD =0.5.

4.2 Sensitivity Analysis

To make it convenient for estimating DSLR under dust aerosol, we discussed the sensitivity of the proposed model. The performance of the proposed DSLR retrieval model depends on the uncertainty of the input variables, mainly for the MODIS instrument detector noise and calibration error, uncertainties in the WVC and AOD, and in the accuracy of the model itself. Several sources of error must be considered to analyze the sensitivity of the proposed model. The total error $e(\Delta DSLR)$ of the proposed method can be expressed as:

$$e(\Delta DSLR) = \sqrt{\delta(L_{DSLR})^2 + \delta(AOD)^2 + \delta(WVC)^2 + \delta(a\lg)^2} \tag{7}$$

with

$$\delta(L_{DSLR}) = \sqrt{\sum a_i^2 \delta M_i^2} \tag{8}$$

$$\delta(AOD) = \left| \frac{\partial \Delta SDLR_{AOD}}{\partial AOD} \Delta(AOD) \right| \tag{9}$$

$$\delta(WVC) = \left| \frac{\partial \Delta SDLR_{AOD}}{\partial WVC} \Delta(WVC) \right| \tag{10}$$

in which $\Delta(AOD)$ and $\Delta(WVC)$ are the uncertainty of the WVC and AOD, respectively, and $\delta(L_{SDLR})$, $\delta(AOD)$ and $\delta(WVC)$ are the errors induced by the uncertainty of the corresponding parameters. According to Remer et al [53], on the global scale, the uncertainty of the AOD for land is :

$$\Delta(AOD) = \pm 0.05 \pm 0.15 AOD \tag{11}$$

Preprints (www.preprints.org) | NOT PEER-REVIEWED | Posted: 12 December 2016 doi:10.20944/preprints201612.0064.v1

Peer-reviewed version available at Remote Sens. 2017, 9, 207; doi:10.3390/rs9030207

And $\delta(AOD)$ can be calculated by using formula (8). Considering that the MODIS TOA brightness temperature error in channels 28, 33, 34 and 35 are 0.25K, 0.05 K for channels 29, 31 and 32, and 0.35 K for channel 36, $\delta(L_{SDLR})$ can be acquired with formula (7). Here, we adopted an uncertainty of the WVC for MODIS product of 0.5 g/cm² [54], so the corresponding $DSLR_{AOD}$ errors for VZA=0° and z=0 km are as follow:

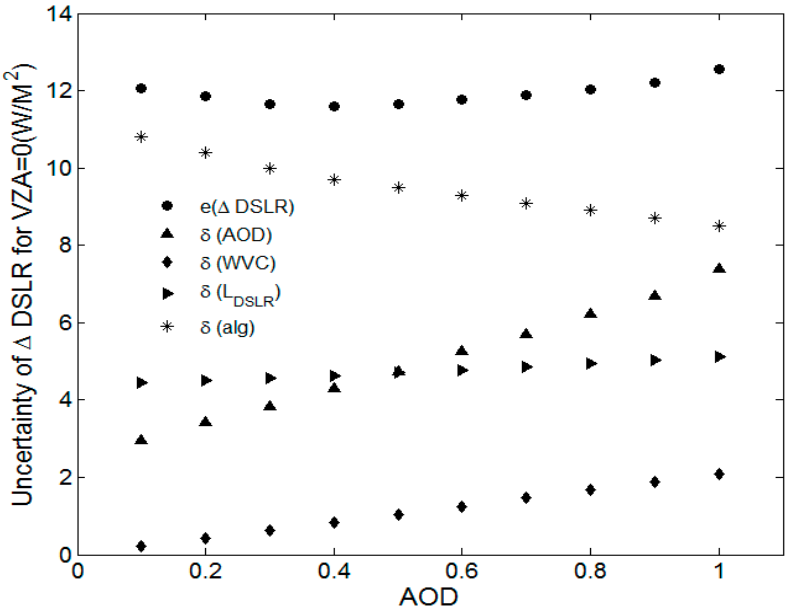

Figure 10. The $DSLR_{AOD}$ error caused by uncertainties of thermal channels, AOD, WVC and the accuracy of the DSLR-GC model for VZA = 0° and DEM=0 km.

From figure 10, it is clear that the $\delta(L_{DSLR})$, $\delta(AOD)$ and $\delta(WVC)$ errors caused by the uncertainty of thermal channel radiance, AOD and WVC increased with the increasing of AOD, but the accuracy of the model itself decreased, which means that the proposed model is more suitable for heavy dust aerosol. Because the $\delta(AOD)$ error has a large proportion and higher tendency, the total error of the proposed algorithm therefore decreased slightly and then increased with increasing AOD. The minimum value is at approximately AOD=0.4. It means that the more accurate AOD should be used when estimating the DSLR under dust aerosol with the proposed method. Because the errors from different variables can be neutralized, the actual values are usually smaller than the corresponding values. The total error $e(\Delta DSLR)$ has a similar tendency for other VZAs and the max value is 16.7 W/M² for VZA = 60° and DEM=0 km when AOD=1.0. The improved model has good performance in estimating the DSLR under heavy dust aerosol.

5. Validations with In-Situ Measurements

It is important to note that the MODIS aerosol product monitors the AOD over part of the continents. Daily Level 2 data are produced at the spatial resolution of a 10x10 1-km (at nadir)-pixel array. MOD04_L2 and MYD04_L2 contain data collected from Terra and Aqua, respectively. The DSLR with the measured time closest to the MODIS Terra/Aqua overpass time was extracted to represent the equivalent DSLR for the pixel scale. As the maximum time interval between MODIS and in situ measurements is 15 minutes, the error caused by the time inconsistency can be ignored. To eliminate the influence of cloud contamination, only the pixels identified as cloud-free were selected.

The objective of the present work is to estimate the instantaneous DSLR under dust aerosol using the proposed method. Only the pixels identified as clear sky were selected based on the quality control data in the MODIS LST MOD11_L2/MYD11_L2 products, from which the dust aerosol sky data were chosen in this study. Figure 11 shows the scattering diagram of the in situ DSLR and the DSLR extracted from MODIS data. The solid circles represent the DSLR estimated using the proposed

Preprints (www.preprints.org) | NOT PEER-REVIEWED | Posted: 12 December 2016 doi:10.20944/preprints201612.0064.v1

Peer-reviewed version available at Remote Sens. 2017, 9, 207; doi:10.3390/rs9030207

model and the hollow circles show that estimated using the DSLR-GC model. The scattering diagrams of the AOD, as a function of the DSLR at the time of MODIS overpass for the two sites, are also shown in Figure 11.

At the Yingke site, most of the dust aerosols occur in spring and autumn, with 118 days of corresponding data for Terra and 89 days for Aqua. The RMSEs of the proposed model are 20.4 W/M² and 24.2 W/M² for Terra and Aqua, respectively, and the biases are 2.7 W/M² and 9.6 W/M², respectively. For the Arvaikheer site, there are 39 days of corresponding data for Terra and 34 days for Aqua, and most dust aerosols occur in spring and early summer or autumn. The RMSEs of the proposed model are 23.2 W/M² and 19.8 W/M² for Terra and Aqua, respectively, and the biases are 7.8 W/M² and 10.5 W/M², respectively. Notably, the RMSEs of the proposed model at the two sites are higher than those in the simulated data. Considering that the ground data measured at the two sites use a point-based scale, whereas the retrieved value from MODIS data using our proposed method corresponds to a spatial resolution of 1 km, if the point-based data are assumed to represent the 1-km spatial scale value for comparison with the value derived from MODIS data, it may lead to large discrepancies if the ground stations are located in a heterogeneous area. Moreover, we assumed that the DSLR error caused by the time inconsistency can be ignored, but the DSLR may change over the time series, especially when there are winds and thin clouds.

In addition to these error factors, the performance of the proposed method is also affected by the quality of the input variable of TOA radiance and uncertainties in the AOD and WVC. The coefficients in the improved model are determined from the datasets simulated using MODTRAN that do not consider polarization in the radiative transfer process for heavy dust aerosol loadings. Moreover, the optical properties of aerosol particles are highly variable in time and space. Differences in the optical properties of the dust aerosol at the two test sites and the average conditions of dust aerosol in OPAC used in this study may also affect the results.

In general, compared with the dust aerosol-free model, the improved model is particularly applicable to acquire relatively high-precision DSLR under heavy dust aerosol from MODIS data for which qualified WVC and AOD are available. The DSLR estimated using the improved model is higher than that estimated using the dust aerosol-free model, especially in high AOD conditions, which may be the reason that the ALRF and correction coefficients are considered in the former. There are few differences when the AOD is lower than 0.2, it may be the reasons that dust aerosols have little influence on the DSLR and the ALRF is small in these conditions.

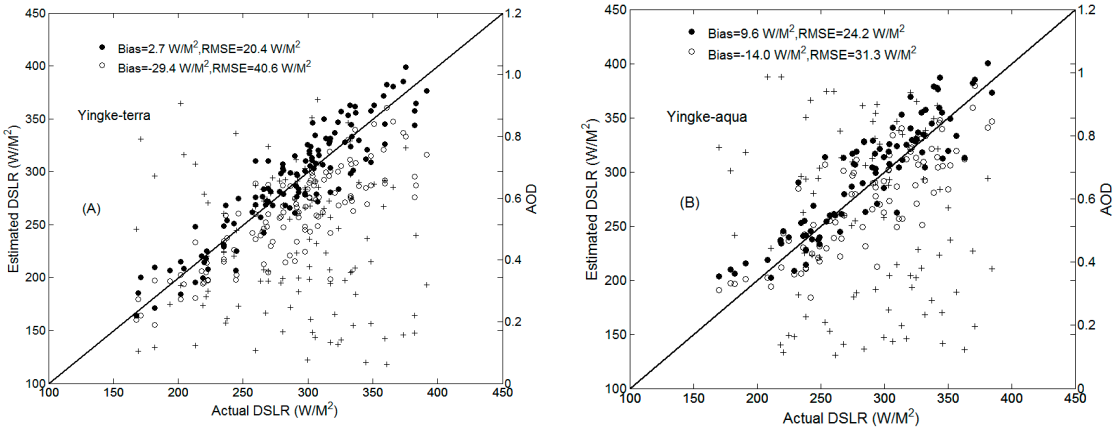

Preprints (www.preprints.org) | NOT PEER-REVIEWED | Posted: 12 December 2016 doi:10.20944/preprints201612.0064.v1

Peer-reviewed version available at Remote Sens. 2017, 9, 207; doi:10.3390/rs9030207

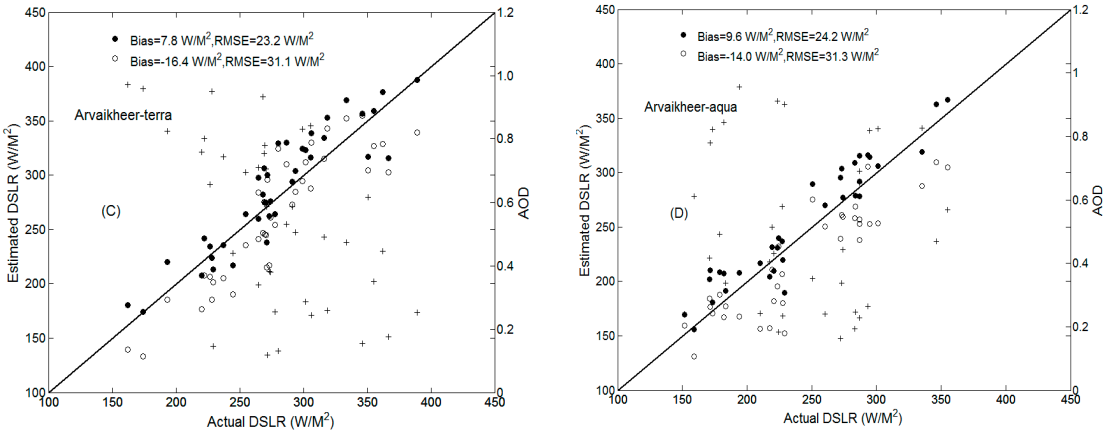

Figure 11. Comparison between the DSLR estimated using the proposed (red solid circles) and DSLR-GC methods (blue hollow circles) and those measured in situ at two test sites for dust aerosol conditions at the moment of MODIS overpass. The scattering diagrams of the AOD (green hollow stars) as function of the actual DSLR are also shown.

6. Conclusions

In this paper, a method has been proposed for estimating DSLR from remotely sensed data for the cloud-free skies under heavy dust aerosol conditions. The AOD and atmospheric WVC were used as explicit inputs to reduce the effect of dust aerosol on the estimation of DSLR. Influence of VZA on the method was also discussed using the simulated data. For VZA =0°, the RMSEs of the proposed model varied from 5.75 W/M² to 8.68 W/M² for different surface types. For VZA =60°, the RMSEs varied from 10.69 W/M² to 12.73 W/M². The RMSE of the proposed model increased as the VZA increased, which indicates that the model is VZA-dependent. As the effect of surface types on the estimated DSLR was slightly the proposed method did not account for the influence associated with different land covers.

Some in-situ field measurements at the Yingke site, China and the Arvaikheer site, Mongolia, were used to validate the proposed method. The results showed that the RMSEs of the retrieved DSLR with the proposed method and the site values were 20.4 W/M² and 24.2 W/M² for Terra and Aqua, respectively, at the Yingke site, and the biases were 2.7 W/M² and 9.6 W/M², respectively. For the Arvaikheer site, the RMSEs were 23.2 W/M² and 19.8 W/M², and the biases were 7.8 W/M² and 10.5 W/M², for Terra and Aqua, respectively. The proposed method is particularly applicable to MODIS data to acquire high accurate DSLR under heavy dust aerosol for which qualified WVC and AOD are available.

Acknowledgments

This work was supported in part by the National Key Research and Development Program of China (NO.2016YFA0600103), in part by the National Natural Science Foundation of China under Grant 41571353 and Grant 41231170, and in part by the Innovation Project of LREIS (O88RA801YA).

Author Contributions

Chunlei Wang wrote the manuscript and conducted data simulations and data analysis. Bo-Hui Tang was in charge of the research design and analysis. Zhao-Liang Li performed the remotely-sensed data processing. Hua Wu and Ronglin Tang collected and analyzed the in situ measurement data.

Conflicts of Interest

The authors declare no conflict of interest.

References

1. Forman, B. A., & Margulis, S. A. High-resolution satellite-based cloud-coupled estimates of total downwelling surface radiation for hydrologic modelling applications. *Hydrology & Earth System Sciences,* **2009**, *13(7)*, 969-986.

Preprints (www.preprints.org) | NOT PEER-REVIEWED | Posted: 12 December 2016 doi:10.20944/preprints201612.0064.v1

Peer-reviewed version available at Remote Sens. 2017, 9, 207; doi:10.3390/rs9030207

2. Tang, B.-H, Li, Z.-L., & Zhang, R. A direct method for estimating net surface shortwave radiation from modis data. *Remote Sensing of Environment*, **2006**, *103(1)*, 115-126.
3. Ohmura, A. Physical basis for the temperature-based melt-index method. *Journal of Applied Meteorology*, **2001**, *40(4)*, 753-761.
4. Meetschen, D., van den Hurk, Bart J. J. M., Ament, F., & Drusch, M. Optimized surface radiation fields derived from meteosat imagery and a regional atmospheric model. *Journal of Hydrometeorology*, **2004**, *5(6)*, 1091.
5. Brunt, D. Notes on radiation in the atmosphere. I. *Quarterly Journal of the Royal Meteorological Society*, **1932**, *58(247)*, 389-420.
6. Brutsaert, W. On a derivable formula for long-wave radiation from clear skies. *Water Resources Research*, **1975**, *11(5)*, 742-744.
7. Duarte, H. F.; Dias, N. L.; Maggiotto, S. R. Assessing daytime downward longwave radiation estimates for clear and cloudy skies in Southern Brazil. *Agricultural and forest meteorology*, **2006**, *139(3)*, 171-181.
8. Iziomon, M. G.; Mayer, H.; Matzarakis, A. Downward atmospheric longwave irradiance under clear and cloudy skies: Measurement and parameterization. *Journal of Atmospheric and Solar-Terrestrial Physics*, **2003**, *65(10)*, 1107-1116.
9. Konzelmann, T.; Wal, R. S.; Greuell, W.; Bintanja, R.; Henneken, E. A.; Abe-Ouchi, A.Parameterization of global and longwave incoming radiation for the greenland ice sheet. *Global & Planetary Change*, **1994**, *9(1–2)*, 143-164.
10. Santos, C. A. C. D.; Silva, B. B. D.; Rao, T. V. R.; Satyamurty, P.; Manzi, A. O. Downward longwave radiation estimates for clear-sky conditions over northeast Brazil. *Revista Brasileira de Meteorologia*, **2011,** *26(3)*, 443-450.
11. Garrett, T. J.; Radke, L. F.; Hobbs, P. V. Aerosol effects on cloud emissivity and surface longwave heating in the arctic. *Journal of the Atmospheric Sciences*, **2010**, *59(3)*, 769-778.
12. Dan, L.; Vogelmann, A. M. A climatologically significant aerosol longwave indirect effect in the Arctic. *Nature*, **2006**, *439(439)*, 453-6.
13. Meloni, D.; Sarra, A. D.; Iorio, T. D. & Fiocco, G. Influence of the vertical profile of saharan dust on the visible direct radiative forcing. *Journal of Quantitative Spectroscopy & Radiative Transfer*.**2005**, *93(4)*, 397-413.
14. Derimian, Y.; Karnieli, A.; Kaufman, Y. J.; et al. Dust and pollution aerosols over the Negev desert, Israel: Properties, transport, and radiative effect. *Journal of Geophysical Research*, **2006,** *111(D5)*, 769-785.
15. Toledano, C.; Cachorro, V. E.; Frutos, A. M. D.; et al. Inventory of African desert dust events over the southwestern Iberian Peninsula in 2000–2005 with an AERONET Cimel Sun photometer. *Journal of Geophysical Research*, **2007**, *112(112)*, 88-97.
16. Saha, A.; Mallet, M.; Roger, J. C.; Dubuisson, P.; Piazzola, J.; Despiau, S. One year measurements of aerosol optical properties over an urban coastal site: effect on local direct radiative forcing.*Atmospheric Research*, **2008**, *90(2–4)*, 195-202.
17. Biagio, C. D.; Sarra, A. D.; Meloni, D.; Monteleone, F.; Piacentino, S.; Sferlazzo, D. Measurements of mediterranean aerosol radiative forcing and influence of the single scattering albedo. *Geochimica Et Cosmochimica Acta*, **2009**, *73(13)*, 605-617.
18. Sicard, M.; Mallet, M.; Garcíavizcaíno, D.; Comerón, A.; Rocadenbosch, F.; Dubuisson, P.; et al. Intense dust and extremely fresh biomass burning outbreak in barcelona, spain: characterization of their optical properties and estimation of their direct radiative forcing.*Environmental Research Letters*, **2012**, *7(3)*, 34016-34021(6).
19. Mccalla, A.Evaluation of the desert dust effects on global, direct and diffuse spectral ultraviolet irradiance. *Tellus Series B-chemical & Physical Meteorology*, **2013**, *65(1)*, 280-280.
20. Esteve, A. R.; Estellés, V.; Utrillas, M. P.; Martínez-Lozano, J. A. Analysis of the aerosol radiative forcing over a mediterranean urban coastal site. *Atmospheric Research*, **2014**, *137(2)*, 195-204.
21. Valenzuela, A.; Olmo, F. J.; Lyamani, H.; Antón, M.; Quirantes, A.; Aladosarboledas, L. Aerosol radiative forcing during african desert dust events (2005–2010) over southeastern Spain. *Atmospheric Chemistry & Physics*, **2012**, *12(21)*, 10331-10351.
22. Sarra, A. D.; Biagio, C. D.; Meloni, D.; Monteleone, F.; Pace, G.; Pugnaghi, S.; et al. Shortwave and longwave radiative effects of the intense saharan dust event of 25–26 march 2010 at lampedusa (mediterranean sea). *Journal of Geophysical Research*, **2011**, *116(D23)*, 2053-2056.
23. Perrone, M. R.; Tafuro, A. M.; Kinne, S. Dust layer effects on the atmospheric radiative budget and heating rate profiles. *Atmospheric Environment*, **2012**, *59(7)*, 344-354.

Preprints (www.preprints.org) | NOT PEER-REVIEWED | Posted: 12 December 2016 doi:10.20944/preprints201612.0064.v1

Peer-reviewed version available at Remote Sens. 2017, 9, 207; doi:10.3390/rs9030207

24. Sicard, M.; Bertolín, S.; Mallet, M.; Dubuisson, P.; Comerón, A. Estimation of mineral dust longwave radiative forcing: sensitivity study to particle properties and application to real cases over Barcelona Atmos. Chem. *Phys. Discuss.*, **2014**,*14*, 8533–8573
25. Obregón M A, Pereira S, Salgueiro V, et al. Aerosol radiative effects during two desert dust events in August 2012 over the Southwestern Iberian Peninsula. *Atmospheric Research*, **2015**, *153*,404-415.
26. Xin J, Gong C, Wang S, et al. Aerosol direct radiative forcing in desert and semi-desert regions of northwestern China. *Atmospheric Research*, **2016**, *171*, 56-65.
27. Zhang, J.; Christopher, S. A. Longwave radiative forcing of saharan dust aerosols estimated from modis, misr, and ceres observations on terra. *Geophysical Research Letters*, **2003**, *30(23)*, 343-354.
28. Haywood, J. M.; Allan, R. P.; Culverwell, I.; Slingo, T.; Milton, S.; Edwards, J.; et al. Can desert dust explain the outgoing longwave radiation anomaly over the sahara during july 2003?. *Journal of Geophysical Research*, **2005**, *110(D5)*, 781-797.
29. Slingo, A.; Ackerman, T. P.; Allan, R. P.; Kassianov, E. I.; Mcfarlane, S. A.; Robinson, G. J.; et al. Observations of the impact of a major saharan dust storm on the atmospheric radiation balance.*Geophysical Research Letters*, **2006**, *21(24)*, 409-421.
30. Thomas, M., Gautier, C., & Ricchiazzi, P. (2009). Investigations of the march 2006 african dust storm using ground-based column-integrated high spectral resolution infrared (8–13 μm) and visible aerosol optical thickness measurements: 1. measurement procedures and results.*Journal of Geophysical Research Atmospheres*, **2009**, *114(D14)*, 1013-1033.
31. Brindley, H. E.; Russell, J. E. An assessment of saharan dust loading and the corresponding cloud-free longwave direct radiative effect from geostationary satellite observations. *Journal of Geophysical Research Atmospheres*, **2009**, *114(D23)*, 1470-1478.
32. Osborne, S. R.; Baran, A. J.; Johnson, B.T.; Haywood, J. M.; Hesse, E.; Newman,S. Short-wave and long-wave radiative properties of saharan dust aerosol. *Quarterly Journal of the Royal Meteorological Society*, **2011**, *137(658)*, 1149-1167.
33. Köhler, C. H.; Trautmann, T.; Lindermeir, E.; Vreeling, W.; Lieke, K.; Kandler, K.; et al. Thermal IR radiative properties of mixed mineral dust and biomass aerosol during samum-2. *Tellus Series B-chemical & Physical Meteorology*, **2011,** *63(4)*, 751–769.
34. Myhre, G.; Grini, A.; Haywood, J. M.; Stordal, F.; Chatenet, B.; Tanré, D.; Isaksen, I. S. Modeling the radiative impact of mineral dust during the Saharan Dust Experiment (SHADE) campaign. *Journal of Geophysical ResearchAtmospheres*, **2003**, *108(D18)*, 203-221.
35. Kaufman,Y.J.; Tanré,D.;Boucher,O. A satellite view of aerosols in the climate system. *Nature*, **2002**, *419(6903)*, 215–223.
36. Dubovik, O.; Holben, B.; Eck, T. F.; Smirnov, A.; Kaufman, Y. J.; King, M. D.; et al. Variability of absorption and optical properties of key aerosol types observed in worldwide locations. *Journal of the Atmospheric Sciences*, **2002**, *59(3)*, 590-608.
37. Tegen, I.; Lacis, A. A.; Fung, I.. The influence on climate forcing of mineral aerosols from disturbed soils. *Nature*, **1996**, *380(6573)*, 419-422.
38. Zhao, S.; Zhang, H.; Feng, S.; et al. Simulating direct effects of dust aerosol on arid and semi-arid regions using an aerosol–climate coupled system. *International Journal of Climatology*, **2015**, *35(8)*, 1858-1866.
39. Chew, B. N.; Campbell, J. R.; Hyer, E. J.; et al. Relationship between Aerosol Optical Depth and Particulate Matter over Singapore: Effects of Aerosol Vertical Distributions. *Aerosol & Air Quality Research*, **2016**, *16(11)*, 1858-1866.
40. Myhre, G.; Grini, A.; Haywood, J. M.; Stordal, F.; Chatenet, B.; Tanré, D.; et al. Modeling the radiative impact of mineral dust during the Saharan dust experiment (shade) campaign. Journal of Geophysical Research Atmospheres, **2003,** 108(D18), 203-221.
41. Christopher, S. A.; Zhang, J. Shortwave aerosol radiative forcing from modis and ceres observations over the oceans. *Geophysical Research Letters*, **2002**, *29(18)*, 61–64.
42. King, M. D., Kaufman, Y. J., Menzel, W. P., & Tanré, D. Remote sensing of cloud, aerosol, and water vapor properties from the moderate resolution imaging spectrometer (modis). *IEEE Transactions on Geoscience & Remote Sensing*, **1992**, *30(1)*, 2-27.
43. Remer, L. A.; Tanré, D.; Kaufman, Y. J.; Ichoku, C.; Mattoo, S.; Levy, R.; et al. Validation of modis aerosol retrieval over ocean.*Geophysical Research Letters*, **2002**, *29(12)*, MOD3-1-MOD3-4.
44. Chu, D. A.; Kaufman, Y. J.; Ichoku, C.; Remer, L. A.; Tanré, D.; Holben, B. N. Validation of modis aerosol optical depth retrieval over land. *Geophysical Research Letters*, **2002**, *29(12)*, MOD2-1–MOD2-4.

Preprints (www.preprints.org) | NOT PEER-REVIEWED | Posted: 12 December 2016 doi:10.20944/preprints201612.0064.v1

Peer-reviewed version available at Remote Sens. 2017, 9, 207; doi:10.3390/rs9030207

45. Kahn, R., Banerjee, P., & Mcdonald, D. (2001). Sensitivity of multi-angle imaging to natural mixtures of aerosols over ocean. *Journal of Geophysical Research Atmospheres*, **2001**, *106(D16)*, 18219-18238.
46. Berk, A.; Anderson, G. P.; Acharya, P. K. et al. MODTRAN 5: a reformulated atmospheric band model with auxiliary species and practical multiple scattering options: update. *Proceedings of SPIE-The International Society for Optical Engineering*, **2005**, *5806*, 662-667.
47. Hess, M., Koepke, P., & Schult, I. Optical properties of aerosols and clouds: the software package opac. *Bulletin of the American Meteorological Society*, **1901**, *79(5)*, 831-844.
48. Ge, J. M.; Su, J.; Ackerman, T. P.; Fu, Q.; Huang, J. P.; Shi, J. S. Dust aerosol optical properties retrieval and radiative forcing over northwestern china during the 2008 China-U.S. joint field experiment.*Journal of Geophysical Research Atmospheres*, **2010**,*115(D7)*, 1154-1157.
49. Tang, B.-H., Li, Z.-L. Estimation of instantaneous net surface longwave radiation from MODIS cloud-free data. *Remote Sensing of Environment*, **2008**, *112(9)*, 3482-3492.
50. Wang, W.; Liang, S. Estimation of high-spatial resolution clear-sky longwave downward and net radiation over land surfaces from MODIS data. *Remote sensing of environment*, **2009**, *113(4)*, 745-754.
51. Wang, K.; Liang, S. Global atmospheric downward longwave radiation over land surface under all-sky conditions from 1973 to 2008.*Journal of Geophysical Research Atmospheres*, **2009**,*114(D19)*, 5274-5274.
52. Wilson, D. J.; Geabanacloche, J. Simple model to estimate the contribution of atmospheric co2 to the earth's greenhouse effect.*American Journal of Physics*, **2012**, *80(4)*, 306-315.
53. Remer, L. A.; Kaufman, Y. J.; Tanré, D.; Mattoo, S.; Chu, D. A.; Martins, J. V.; et al. The MODIS aerosol algorithm, products, and validation. *Journal of the Atmospheric Sciences*, **2005**, *62(4)*, 947-973.
54. Sobrino, J. A.; Kharraz,J.; Li, Z.-L.Surface temperature and water vapor retrieval from MODIS data. *International Journal of Remote Sensing*, **2003**, *24(24)*, 5161-5182.

© 2016 by the authors; licensee Preprints, Basel, Switzerland. This article is an open access article distributed under the terms and conditions of the Creative Commons by Attribution (CC-BY) license (http://creativecommons.org/licenses/by/4.0/).